Applied Mathematical Modelling 34 (2010) 1559–1573

Contents lists available at ScienceDirect

Applied Mathematical Modelling

journal homepage: www.elsevier.com/locate/apm

A numerical simulation of unsteady blood flow through multi-irregular arterial stenoses

Norzieha Mustapha [a,*], Prashanta K. Mandal [b], Peter R. Johnston [c], Norsarahaida Amin [a]

[a] Department of Mathematics, Faculty of Science, Universiti Teknologi Malaysia, Malaysia
[b] Department of Mathematics, Visva-Bharati, Santiniketan 731 235, India
[c] Department of Mathematics, Griffith University, Australia

ARTICLE INFO

Article history:
Received 21 April 2008
Received in revised form 27 August 2009
Accepted 1 September 2009
Available online 12 September 2009

Keywords:
Multi-irregular stenoses
Computational fluid dynamics
Flow separation
Wall shear stress

ABSTRACT

An unsteady mathematical model to study the characteristics of blood flowing through an arterial segment in the presence of a couple of stenoses with surface irregularities is developed. The flow is treated to be axisymmetric, with an outline of the stenoses obtained from a three dimensional casting of a mildly stenosed artery [1], so that the flow effectively becomes two-dimensional. The governing equations of motion accompanied by appropriate choice of boundary and initial conditions are solved numerically by MAC (Marker and Cell) method in cylindrical polar coordinate system in staggered grids and checked numerical stability with desired degree of accuracy. The pressure-Poisson equation has been solved by successive-over-relaxation (SOR) method and the pressure–velocity correction formulae have been derived. The flexibility of the arterial wall has also been accounted for in the present investigation. Further, in-depth study in the flow pattern reveals that the separation Reynolds number for the multi-irregular stenoses is lower than those for cosine-shaped stenoses and a long single irregular stenosis. The present results predict the excess pressure drop across the cosine stenoses than the irregular ones and show quite consistency with several existing results in the literature which substantiate sufficiently to validate the applicability of the model under consideration.

1. Introduction

There is evidence that cardiovascular stenotic flows as well as vascular wall deformability play important roles in the development and progression of arterial stenosis, one of the most widespread diseases in human beings, leading to the malfunction of the cardiovascular system. Some researchers have the opinion that the damage to the inner coating of the artery, the intima, is responsible for the initial formation of stenosis [2] and also for regrowth of the stenosis after balloon angiography [3]. It has been established that once a mild stenosis is developed, the resulting flow disorder further influences the development of the disease and arterial deformability, and changes the regional blood rheology, as well [4].

Because of the fact that real atherosclerotic lesions are asymmetric and irregular [1], we need to have better understanding factor controlling blood flow in such constricted geometries. In general, the surface irregularities of the stenosis add complexity to experimental and numerical simulations of the flow phenomena. Keeping in view such complexities, a great amount of scientific effort has already been invested on investigating the flow characteristics of blood through occluded vessels [5–12]. Johnston and Kilpatrick [5] obtained in their findings that the highest pressure drop was noted across the cosine-shaped stenosis rather than the irregularly-shaped stenosis throughout the entire range of Reynolds numbers and concluded

* Corresponding author.
E-mail address: norzieha@mel.fs.utm.my (N. Mustapha).

0307-904X/$ - see front matter © 2009 Elsevier Inc. All rights reserved.
doi:10.1016/j.apm.2009.09.008

that the smoothness factor was the prime cause for such behaviour. In a bid to "verify or disprove" the findings of [5], Andersson et al. [6] were inclined to draw the conclusion that the pressure drop across the stenosed artery is practically unaffected by surface irregularities at low Reynolds number and they also demonstrated that the high flow resistance predicted across the cosine-shaped stenosis is a consequence of its symmetry and not due to its smooth surface, while the irregular stenosis geometry exhibits an asymmetric shape which tended to reduce the pressure drop. Finally, they concluded that the degree of stenosis asymmetry is at least equally important as the presence of surface irregularities. Yakhot et al. [7] in their extensive simulation using an immersed-boundary method, explored the influence of the shape and surface roughness on the flow resistance and found that surface irregularities had no significant influence on the flow resistance across an obstacle for a physiological range of Reynolds numbers. They agree with Andersson et al. [6] that the pressure drop excess across the cosine-shaped stenosis is a consequence of the particular geometrical shape of the stenosis and is unaffected by stenosis surface roughness. In their findings, they concluded that the narrowest cross-section of the cosine-shaped stenosis caused higher occlusion of the vessel and, consequently, higher flow resistance. In conformity with the findings of [5–7], Chakravarty et al. [8] concluded that flowing blood experiences much higher resistance to flow in the presence of a cosine-shaped stenosis than irregular model. In a numerical study based on finite volume algorithm for flow through complicated geometries, Politis et al. [9,10] demonstrated in their simulation on composite arterial coronary grafts that the local hemodynamics (described by velocity, pressure drop, wall shear stress and flow rates) are strongly influenced by the local geometry, specially at the anastomotic sites and they also concluded that sites of lowest shear stress regions (the lateral walls of bifurcations) are susceptible to the occurrence of coronary artery disease [9] while in transient flow simulation by a finite-volume method, the process of restenosis has been successfully carried out by employing different grafting distances and various inflow rate ratios [10]. In another study on pulsatile flow in composite arterial coronary grafts, Politis et al. [11] concluded that the time-varying physiological flow rate through the composite arterial coronary grafts produces a more disturbed flow than a pure sinusoidal flow, specially at peak cardiac systole. They are also of the opinion that wide region of recirculation zones along with stagnation flow occur at peak systole. Intracoronary flow through an anatomically accurate 3D coronary arterial tree from an explanted porcine heart by excluding coronary motion was successfully carried out both experimentally as well as computationally by Boutsianis et al. [12]. They concluded that the areas of amplified variations in wall shear stress, mostly evident in the neighbourhoods of arterial branching, seem to correlate well with clinically observed increased atherogenesis and the intracoronary flow lines showed stasis and extreme vorticity during the phase of minimum coronary flow in contrast to streamlined undisturbed flow during the phase of maximum flow. Recently, effects of surface roughness of stenosis on blood flow have been successfully carried out by Sarifuddin et al. [13–15] and Mandal et al. [16].

Owing to the existence of multiple sites of narrowing into the arterial lumen, Seeley and Young [17] studied the pressure drop across multiple stenoses by considering two blunt plugs in series and opined that, in general, the pressure drop cannot be obtained by a summation of pressure drops for single stenosis since the proximal and distal stenoses "interfere" with each other unless the spacing between them exceeds some critical distance depending on Reynolds number. Meanwhile, Talukder et al. [18] indicated that the total effect of a series of noncritical stenoses is approximately equal to the sum of their individual effects and that the combined effect of series of noncritical stenoses thus can be critical. They suggested that the flow energy loss due to the presence of the stenoses, which is directly related to the pressure drops across them, increases with the number of stenoses and is not strongly dependent on the spacing between them. Dreumel and Keiken [19] opined that the pressure drop across two identical (62%) stenoses equals to that of two single stenoses for low Reynolds numbers. Their observation also predicts the excess pressure drop for a long single stenosis compared with double stenoses of the same length with the distance in between. Kilpatrick et al. [20] presented an approximate assessment of the combined effect by summing the value of the resistance for each stenoses, but not by the degree of the stenoses. They also opined that if one stenosis is more severe than the other, the combined effect can be regarded as same as the effect of the more severe stenosis acting by itself. The distance between the stenoses does not change their combined effect. Gould and Lipscomb [21] and Sabbah and Stein [22] concluded that multiple stenoses produce more resistance to flow than a single stenosis of similar length. Multiple stenoses would be expected to have a greater impact on flow than a single stenosis of similar total length, owing to the multiple entrance and exit points with increased propensities for flow turbulence as pointed out by Nichols et al. [23].

Fukushima et al. [24] numerically investigated the velocity and wall shear stress distribution in a model with two stenoses. They noted that the head of the velocity profiles in the first constriction was flatter than that in the second constriction and the slope of wall shear stress much greater at the reattachment points in the first diverging section than at the points in the second diverging section. Johnston and Kilpatrick [25] and Ang and Mazumdar [26] simulated the arterial blood flow in paired smooth stenoses and triple smooth stenoses, respectively, using the FIDAP computational fluid dynamics package. They concluded that the more severe stenosis dominates the pair and the recirculation between stenoses is stronger with a severe proximal stenosis than a severe distal stenosis. Dullien and Azzam [27] studied the flow rate-pressure drop through channels with continuous irregular walls experimentally and they observed a reduction in flow rate through channels with wall roughness when compared with the value for a smooth channel of the same mean size. Bertolotti et al. [28] studied the influences of multiple stenoses numerically as well as experimentally to diagnosis peripheral arterial diseases and evaluated the peak systolic velocity ratio (PSVR) and pressure drop to detect and grade multiple stenoses in lower limb mimicking arteries. They are also of the opinion for mutual haemodynamic interaction between two stenoses. Very recently, Mustapha

et al. [29–31] explored the effect of multiple stenoses on the flow characteristics of blood past a couple of irregular arterial constrictions.

Since coronary artery disease may have multiple sites of narrowings, an attempt is made in the present theoretical investigation to develop a mathematical model to explore the characteristics of Newtonian blood flow past a realistic diseased arterial segment. Additionally, experimental observations showed that the deformability of the vessel wall also has a potential contribution to the flow behaviour of blood. This provokes us to consider the effect of arterial wall motion into the flow characteristics of blood. The aim of the present study is to explore the effects of some essential features like the unsteadiness of flow, the flexibility of the arterial wall, the effect of differently shaped stenoses and the influence of multiple stenoses with varying severities compared to a long single stenosis on the flow characteristics of blood. More importantly, one of the objectives of the present investigation is to demonstrate that relatively simple finite difference schemes can be employed to simulate flow in rather complex geometries. The present approach differs considerably from others who have calculated or analysed similar problems by using an immersed boundary method, finite element method, a finite-volume method to handle the irregular stenosis rather than finite difference formulations.

2. Stenosis model

The geometry of the stenosis considered herein is a rough (irregular) stenosis profile, which is constructed from the data developed by Back et al. [1] mimicking real surface irregularities since the actual variation of the cross-sectional area of a left circumflex coronary artery casting from a human cadaver is retained. The second geometrical model of the stenosis (smooth) considered is the conventionally used cosine curve (cf. Fig. 1a):

$$R(z,t)=\begin{cases} a_1(t)\left[1-\frac{\delta_1}{2R_0}\left(1+\cos\left(\frac{\pi(z-S_1)}{Z_1}\right)\right)\right], & S_1-Z_1<z<S_1+Z_1,\\ a_1(t)\left[1-\frac{\delta_2}{2R_0}\left(1+\cos\left(\frac{\pi(z-S_2)}{Z_2}\right)\right)\right], & S_2-Z_2<z<S_2+Z_2,\\ a_1(t), & \text{otherwise}, \end{cases} \tag{1}$$

where $R(z,t)$ is the radius of the artery in stenotic region and R_0, in non-stenotic region. The time-variant parameter is described as

$$a_1(t)=1+k_R\cos(\omega t-\phi) \tag{2}$$

in which $\omega = 2\pi f_p$ is the angular frequency with f_p is the pulse frequency and k_R is a constant. Secondly, we consider a couple of irregular stenoses versus a long single irregular stenosis of similar total length L (cf. Fig. 1b).

3. Governing equations

The streaming blood in the arterial lumen is treated as a homogeneous Newtonian fluid. Introducing a radial coordinate transformation $x=\frac{r}{R(z,t)}$, the Navier–Stokes equations and the equation of continuity that govern the unsteady nonlinear fully developed swirl-free flow of blood may be written in dimensionless form as

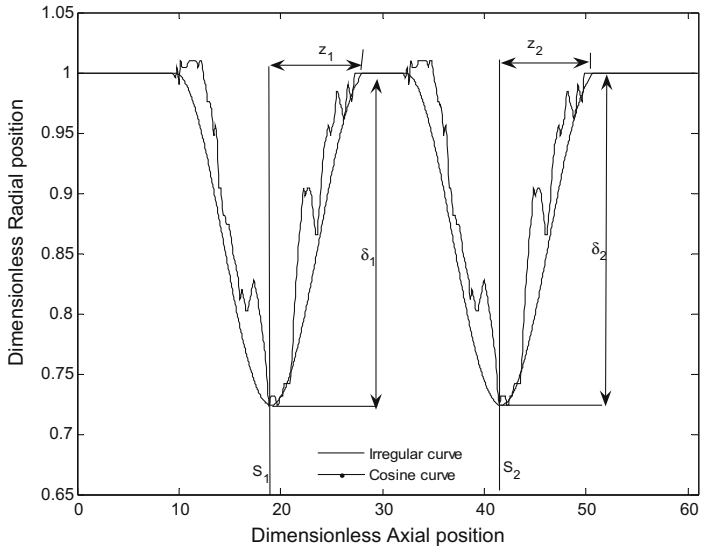

Fig. 1a. Profile of a couple of stenoses.

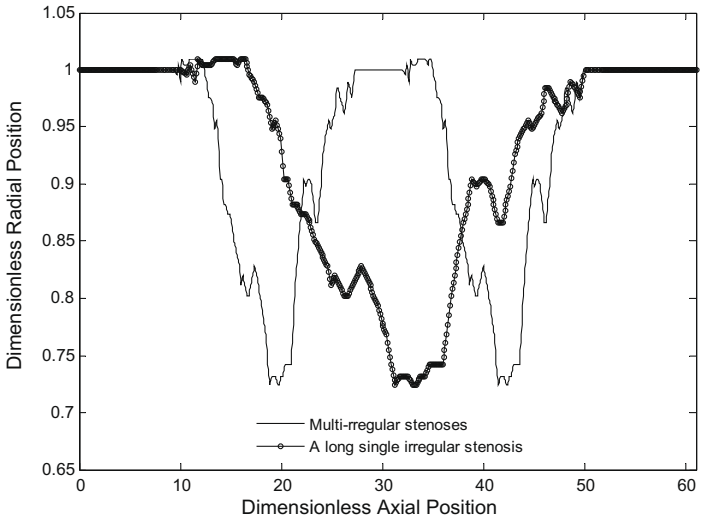

Fig. 1b. Profile of a couple of irregular stenoses and a long single irregular stenosis.

$$\frac{\partial w}{\partial t} = +\frac{x}{R}\frac{\partial R}{\partial t}\frac{\partial w}{\partial x} - \frac{1}{R}\frac{\partial (wu)}{\partial x} - \frac{\partial w^2}{\partial z} + \frac{x}{R}\frac{\partial R}{\partial z}\frac{\partial w^2}{\partial x} - \frac{wu}{xR} - \frac{\partial p}{\partial z} + \frac{x}{R}\frac{\partial R}{\partial z}\frac{\partial p}{\partial x} \times \frac{1}{\mathrm{Re}R^2}\left\{\left[1+\left(x\frac{\partial R}{\partial z}\right)^2\right]\frac{\partial^2 w}{\partial x^2} + \left[\frac{1}{x} + 2x\left(\frac{\partial R}{\partial z}\right)^2 - xR\frac{\partial^2 R}{\partial z^2}\right]\frac{\partial w}{\partial x} + R^2\frac{\partial^2 w}{\partial z^2}\right\}, \tag{3}$$

$$\frac{\partial u}{\partial t} = +\frac{x}{R}\frac{\partial R}{\partial t}\frac{\partial u}{\partial x} - \frac{1}{R}\frac{\partial u^2}{\partial x} - \frac{\partial (wu)}{\partial z} + \frac{x}{R}\frac{\partial R}{\partial z}\frac{\partial (wu)}{\partial x} - \frac{u^2}{xR} - \frac{1}{R}\frac{\partial p}{\partial x} \times \frac{1}{\mathrm{Re}R^2}\left\{\left[1+\left(x\frac{\partial R}{\partial z}\right)^2\right]\frac{\partial^2 u}{\partial x^2} + \left[\frac{1}{x} + 2x\left(\frac{\partial R}{\partial z}\right)^2 - xR\frac{\partial^2 R}{\partial z^2}\right]\frac{\partial u}{\partial x} - \frac{u}{x^2} + R^2\frac{\partial^2 u}{\partial z^2}\right\}, \tag{4}$$

$$xR\frac{\partial w}{\partial z} - x^2\frac{\partial w}{\partial x}\frac{\partial R}{\partial z} + \frac{\partial (ux)}{\partial x} = 0, \tag{5}$$

where r and z are the dimensionless coordinates, scaled with respect to r_0, with the z-axis located along the symmetry axis of the artery. As there is no secondary or rotational flow, so the total velocity is defined by dimensionless radial and axial components, u and w scaled with respect to the cross-sectional average velocity U_0. The Reynolds number Re may be defined as $\mathrm{Re} = U_0 r_0 \rho/\mu$ in which ρ is the density and μ, the viscosity of blood.

The transformed boundary and initial conditions are

$$w(z,x,t) = 0, \quad u(z,x,t) = \frac{\partial R}{\partial t} \quad \text{for } x = 1, \tag{6}$$

$$\frac{\partial w(z,x,t)}{\partial x} = 0 = u(z,x,t) \quad \text{for } x = 0, \tag{7}$$

$$w(z,x,t) = 2(1-x^2), \quad u(z,x,t) = 0 \quad \text{for } z = 0, \tag{8}$$

$$\frac{\partial w(z,x,t)}{\partial z} = 0 = \frac{\partial u(z,x,t)}{\partial z} \quad \text{for } z = L, \tag{9}$$

$$\text{and lastly,} \quad w(z,x,0) = u(z,x,0), \quad p(z,x,0) = 0 \quad \text{for } z > 0. \tag{10}$$

4. Method of solution

The governing Eqs. (3)–(5) along with the set of boundary and initial conditions (6)–(10) are solved numerically by finite difference method in a staggered grid, normally known as MAC (Marker and Cell) method. In this type of grid alignment, the flow velocity field and the pressure are calculated at different locations of control volume as indicated in Fig. 2 while the difference equations have been derived in three distinct cells corresponding to the continuity Eq. (5), the axial momentum (3) and the radial momentum (4) equations. The discretizations of the time derivatives terms are based on the first order accurate two-level forward time differencing formula while those for the convective terms in the momentum equations are accorded with a hybrid formula consisting of central differencing and second order upwinding. The diffusive terms are, however, discretized with second order accurate three-point central difference formula. Thus, in this finite difference

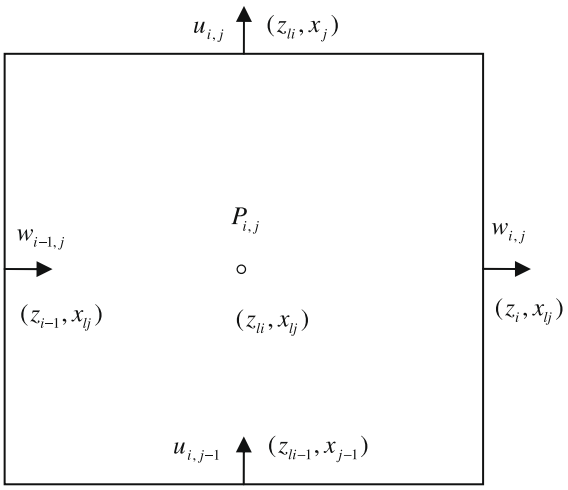

Fig. 2. Typical MAC cell.

formulation, we define $x = j\Delta x$, $z = i\Delta z_i$, $t = k\Delta t$ and $p(z, x, t) = p(i\Delta z_i, j\Delta x, k\Delta t) = p^k_{i,j}$, in which k refers to the time direction, Δt, the time increment, and Δz_i, Δx are the width and length $(i,j)_{th}$ control volume.

The discretized form of the continuity equation at the (i,j) cell takes the form

$$x_{lj}R^k_{li}\left(\frac{w^k_{i,j} - w^k_{i-1,j}}{\Delta z_i}\right) - (x_{lj})^2\left(\frac{\partial R}{\partial z}\right)^k_{li}\left(\frac{w_{at} - w_{ab}}{\Delta x}\right) + \left(\frac{x_j u^k_{i,j} - x_{j-1}u^k_{i,j-1}}{\Delta x}\right) = 0, \tag{11}$$

where

$$w_{at} = 0.25(w^k_{i,j} + w^k_{i-1,j} + w^k_{i-1,j+1} + w^k_{ij+1}), \tag{12}$$

$$w_{ab} = 0.25(w^k_{i,j} + w^k_{i-1,j} + w^k_{i,j-1} + w^k_{i-1,j-1}), \tag{13}$$

$$x_{lj} = x_j - \frac{\Delta x}{2}, \quad R^k_{li} = R(z_{li}), \quad z_{li} = z_i - \frac{\Delta z_i}{2}. \tag{14}$$

Here (z_{li}, x_{lj}) and (z_i, x_j) represent the respective coordinates of the cell center and the cell top right corner of the control volume.

The axial momentum equation may be put to the form as

$$\left(\frac{w^{k+1}_{i,j} - w^k_{i,j}}{\Delta t}\right) = 2\left(\frac{p^k_{i,j} - p^k_{i+1,j}}{\Delta z_i + \Delta z_{i+1}}\right) + \frac{x_{lj}}{R^k_i}\left(\frac{\partial R}{\partial z}\right)^k_i\left(\frac{p_t - p_b}{\Delta x}\right) + (wme)^k_{i,j}, \tag{15}$$

$$\text{with } p_t = \frac{(p^k_{i,j} + p^k_{i,j+1})\Delta z_{i+1} + (p^k_{i+1,j} + p^k_{i+1,j+1})\Delta z_i}{2(\Delta z_i + \Delta z_{i+1})}, \tag{16}$$

$$p_b = \frac{(p^k_{i,j} + p^k_{i,j-1})\Delta z_{i+1} + (p^k_{i+1,j} + p^k_{i+1,j-1})\Delta z_i}{2(\Delta z_i + \Delta z_{i+1})} \tag{17}$$

and

$$wme^k_{i,j} = \text{Conw}^k_{i,j} + \frac{1}{\text{Re}}(\text{Diff}w^k_{i,j}), \tag{18}$$

where $\text{Conw}^n_{i,j}$, the convective terms and $\text{Diff}w^k_{i,j}$, the diffusive terms of the axial momentum at the nth time level at (i,j) cell – the expressions of which are not presented for the sake of brevity.

Likewise, the finite difference equation approximating the momentum equation in radial direction is given by

$$\left(\frac{u^{k+1}_{i,j} - u^k_{i,j}}{\Delta t}\right) = \frac{1}{R^k_{li}}\left(\frac{p^k_{i,j} - p^k_{i,j+1}}{\Delta x}\right) + ume^k_{i,j}, \tag{19}$$

where

$$ume^k_{i,j} = \text{Conu}^k_{i,j} + \frac{1}{\text{Re}}\text{Diff}u^k_{i,j}. \tag{20}$$

The Poisson equation for pressure, derived from Eqs. (11), (15) and (19) takes the final form as

$$\frac{Div_{i,j}^{k+1}-Div_{i,j}^{k}}{\Delta t}=A_{i,j}p_{i,j}^{k}+B_{i,j}p_{i+1,j}^{k}+C_{i,j}p_{i-1,j}^{k}+D_{i,j}p_{i,j+1}^{k}+E_{i,j}p_{i,j-1}^{k}+F_{i,j}p_{i+1,j+1}^{k}+G_{i,j}p_{i+1,j-1}^{k}$$
$$+H_{i,j}p_{i-1,j-1}^{k}+S_{i,j}p_{i-1,j+1}^{k}+x_{lj}R_{li}^{k}\left(\frac{wme_{i,j}^{k}-wme_{i-1,j}^{k}}{\Delta z_i}\right)+\left(\frac{x_j ume_{i,j}^{k}-x_{j-1}ume_{i,j-1}^{k}}{\Delta x}\right). \tag{21}$$

Here, $Div_{i,j}^{k}$ represents the discretized form of the divergence of velocity field at the (i,j) cell and the expressions for A, B, C, D, E, F, G, H, S have got their respective expressions included in the Appendix. The Poisson equation for pressure (21) is solved iteratively by the successive-over-relaxation method with a certain number of iterations in order to get the intermediate pressure-field at the kth time step. The value of the over-relaxation parameter is taken here as 1.2 to make the maximized rate of convergence of SOR.

4.1. Pressure and velocity corrections

The velocity obtained after solving the momentum equations using an intermediate pressure-field may not satisfy the continuity equation. Thus, the corrector stage is necessary to get a more accurate velocity-field which will satisfy the continuity equation more accurately. The pressure correction formula is

$$p_{i,j}^{k}=p_{i,j}^{*}+\omega_2\Delta p_{i,j}, \tag{22}$$

where $p_{i,j}^{*}$ is obtained after solving the Poisson equation, ω_2 ($\leqslant 0.5$) is an under relaxation parameter and

$$\Delta p_{i,j}=-\frac{Div_{i,j}^{*}}{\Delta t A_{i,j}}. \tag{23}$$

The velocity correction formulas are

$$w_{i,j}^{k+1}=w_{i,j}^{*}+\frac{\Delta t\Delta p_{i,j}}{0.5(\Delta z_{i+1}+\Delta z_i)}, \tag{24}$$
$$w_{i-1,j}^{k+1}=w_{i-1,j}^{*}-\frac{\Delta t\Delta p_{i,j}}{0.5(\Delta z_i+\Delta z_{i-1})}, \tag{25}$$
$$u_{i,j}^{k+1}=u_{i,j}^{*}+\frac{\Delta t\Delta p_{i,j}}{R_{li}\Delta x}, \tag{26}$$
$$u_{i,j-1}^{k+1}=u_{i,j-1}^{*}-\frac{\Delta t\Delta p_{i,j}}{R_{li}\Delta x}, \tag{27}$$

where $w_{i,j}^{*}, w_{i-1,j}^{*}, u_{i,j}^{*}, u_{i,j-1}^{*}$ represent the updated velocity-field.

4.2. Numerical stability

We have chosen a step size of 0.025 along x, while along z it varies due to the irregularities of the stenoses data but the step-size along t is based on the following stability condition [32–34], given by

$$\Delta t=c\,\mathrm{Min}[\Delta t_1,\Delta t_2]_{ij} \tag{28}$$

with

$$\Delta t_1\leqslant \mathrm{Min}\left[\frac{\Delta z_i}{|w|},\frac{\Delta x}{|u|}\right]_{ij}\quad\text{and}\quad \Delta t_2\leqslant \mathrm{Min}\left[\frac{\mathrm{Re}}{2}\frac{\Delta x^2\Delta z_i^2}{(\Delta x^2+\Delta z_i^2)}\right]_{ij}, \tag{29}$$

where $0.2<c<0.5$; the reason for this extra added factor c in (28) led to a considerable computational savings as evident from [34] and our experience concurs with them. Moreover, the upwinding parameter β appearing in the expression of $Conw_{i,j}^{n}$ is selected according to the inequalities

$$1\geqslant\beta\geqslant \mathrm{Max}\left[\left|\frac{w\Delta t}{\Delta z_i}\right|,\left|\frac{u\Delta t}{\Delta x}\right|\right]_{ij}. \tag{30}$$

This inequality yields a very small value of the parameter β. As a safety measure the value is multiplied by a factor 1.2, in practice.

5. Numerical results and discussion

For the purpose of numerical computation of the desired quantities of major physiological significance, the following parameters have been ranged around some typical values in order toobtain results of physiological interest [1,35]:

$$k = 0.0001, \quad \omega = 2\pi f_p, \quad f_p = 1.2\ \text{Hz}, \quad \phi = 0^\circ, \quad \rho = 1.05 \times 10^3\ \text{kg m}^{-3}, \quad r_0 = 0.154\ \text{cm}, \quad U_0 = 0.5, \quad \Delta x = 0.025.$$

The numerical results present in this section are obtained after the steady state is achieved, that is, when the non-dimensional time is 68. The computational domain has been confined with a finite non-dimensional arterial length of 60.6 in which the upstream, between two stenoses and the downstream lengths have been selected to be 8, 2 and 10 times the non-dimensional radius, respectively. For this computational domain, solutions are computed through the generation of staggered grids with a size 979×40 while the insertion of additional points are needed between any two consecutive original irregular stenosis data of Back et al. [1] by interpolation and this has been made for the purpose of generating finer mesh adequately. It is worth pointing out that this simulation (using Matlab) has been carried out on a desktop workstation equipped with Pentium IV, 2.8 GHz processor with 512 MB RAM. On average, the simulation requires 6 h for getting velocity field in steady state.

5.1. Model verification and validation

A few simulations with a finer grid and smaller time-step for the axial velocity profiles downstream the constrictions at Re = 300 are presented in Fig. 3. These simulations concerning the grid independence study were performed for the purpose of examining the error associated with the grid and time step used. One may notice from this figure that the profiles concerning three distinct grid sizes almost get overlapped one with another. Thus the grid independence study in the present context of numerical simulation has its own importance to establish the correctness of the results obtained.

In order to validate the applicability of the model under consideration, we compare our numerical results of the normalized pressure drop obtained for a single irregular stenosis with the experimental results [1] and existing numerical results [6] in Fig. 4. The comparison in Fig. 4 shows considerable agreement with both the experimental measurement [1] and theoretical results [6] with a little variation for rigid arterial segment. Such deviations are in good agreement with Yakhot et al. [7], which results from the responsible treatment of unsteady flow mechanism of the present investigation in refined mesh sizes. The present figure also displays the result for flexible artery predicting higher pressure drop which may be justified in the sense that the excess pressure drop appears due to more area covering for flexible artery with respect to the rigid artery.

5.2. Pressure drop

Pressure drops across a stenosis is due to huge changes of energy in the blood resulting from speed up of blood flow through the critical stenosis. The previous investigation [24] showed that the most important factors which influence the pressure drop across multiple stenoses are the severity of the stenoses, the distance between the two stenoses and the Reynolds numbers. Talukder et al. [18] noted that the flow energy loss due to the presence of the stenoses, which is directly related to the pressure drop across them, increases with the number of stenoses and is not strongly dependent on the spacing between them. Table 1 shows dimensionless normalized pressure drop across a single irregular stenosis and multiple irregular stenoses with the distance between the two stenoses is $2R_0$.

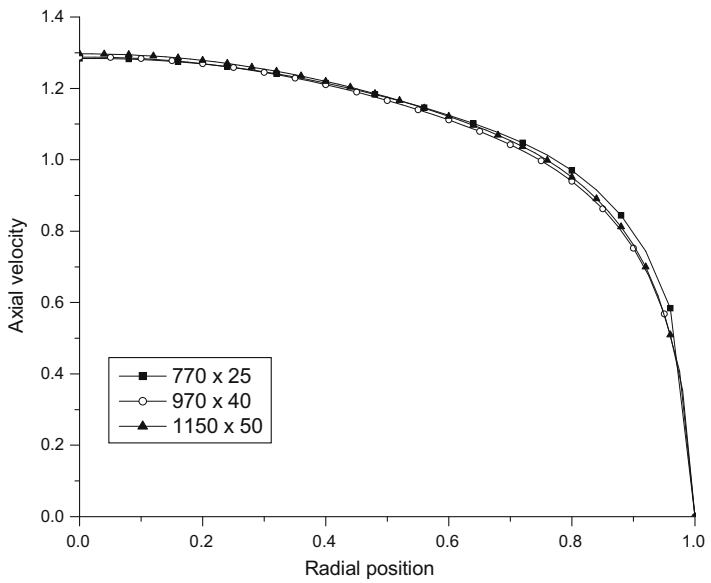

Fig. 3. Variation of the axial velocity profiles for different grid sizes at Re = 300.

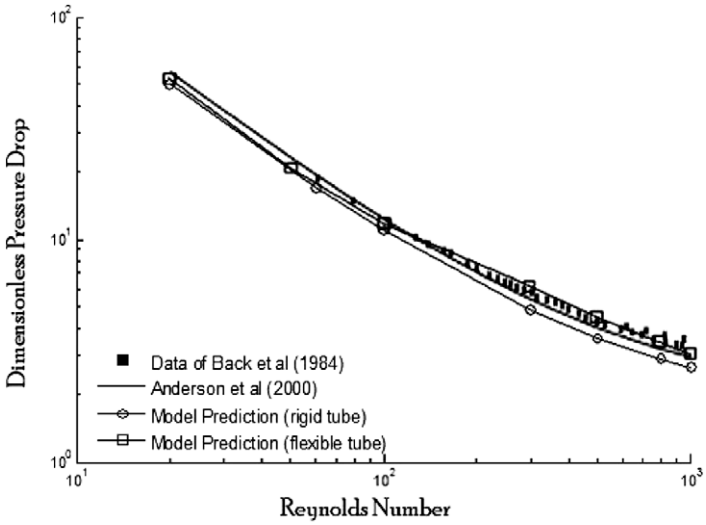

Fig. 4. Comparison of dimensionless pressure drop across a single irregular stenosis.

Table 1
Dimensionless pressure drop across a single and multiple irregular stenoses.

Model of stenosis	Re = 20	Re = 100	Re = 500	Re = 1000
A single-irregular	53.6008	11.7804	4.5152	3.0864
Multi-irregular	102.4716	21.9838	7.0521	5.5042

5.2.1. Multiple irregular stenoses versus cosine stenoses

Observations from Fig. 5 clearly indicate that the normalized pressure drop is for the cosine model excess over irregular model of multiple stenoses. Such observations are in good agreement with those of [6]. On the basis of the present data it may also be noted that the higher value for the cosine-shaped stenoses than the irregular stenoses is due to the increased area covering. Thus contrary to the conclusions of previous studies, the present findings demonstrate along with Yakhot et al.

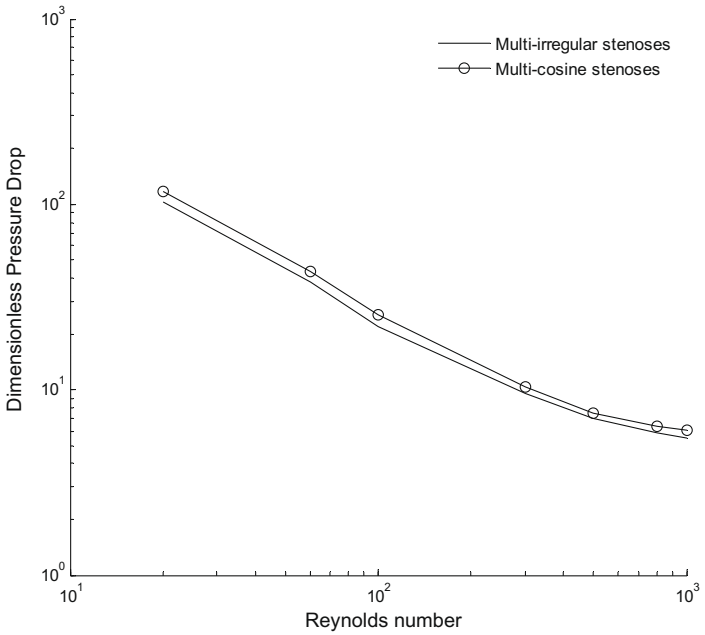

Fig. 5. Dimensionless pressure drop across multiple stenoses with irregular and cosine geometry.

[7] that the excess pressure drop is neither caused by the smoothness of the stenoses nor by its higher degree of symmetry relative to the irregular stenoses, but is rather an effect of area cover.

5.2.2. Multiple irregular stenoses versus a long single irregular stenosis

The dimensionless pressure drops across both the multiple irregular stenoses and a long single irregular stenoses are equal for low Reynolds number while for Reynolds number in between 30 and 100, the dimensionless pressure drop produced by a long single irregular stenosis is about 3.6% higher compared to multi-irregular stenoses of a similar total length as evident from Fig. 6. These results are in good agreement with those of Dreumel and Keiken [19]. However, when the Reynolds numbers are increased up to 1000, the values of dimensionless pressure drops across multiple stenoses exceeds the values for a long single stenosis which in turn produces more resistance to flow.

5.3. Velocity profiles

Fig. 7 shows the cross-sectional profiles of the axial velocity component corresponding to various axial positions in the multi-irregular stenoses at Re = 1000. It appears that the profiles get distorted substantially in the downstream of the narrowest point ($z = 18.8525$ and $z = 41.4525$). Although the height of the narrowest point for these two stenoses are similar, the velocities at the critical height of the first stenosis are higher than second stenosis. From this figure, it can be seen that an almost parabolic profile is retained in the flow upstream which is in good agreement with those of Andersson et al. [6] and Sariffudin et al. [15], who treated the streaming blood through a single irregular stenosis.

The dimensionless centerline velocities for multi-irregular and multi-cosine stenoses at Re = 1000 are presented in Fig. 8. The centerline velocity for multiple-cosine stenoses gives higher values than multiple-irregular stenoses. The conclusion that area cover causes the excess pressure drop across these two geometrically different stenoses models may further be justified from the behaviour of the axial centerline velocity along the axis of each stenosis. This figure also includes one additional curve for a long single stenosis so as to estimate the influence of long single stenosis on the centerline velocity. This result shows that the pressure drop across a long single stenosis is lower than multiple stenosis at Re = 1000 owing to smaller area covering for a long single stenosis.

5.4. Critical Reynolds number

Critical Reynolds number is the minimum Reynolds number that can produce flow separation which can be understood in a sense that the shear stress at the wall becomes zero. The critical Reynolds numbers for three different models of stenoses are shown in Table 2. It is worthwhile to mention that flow separation takes place for lesser Reynolds number when the streaming blood past through a multiple irregular stenoses than multi-cosine and a long irregular stenosis of similar total length.

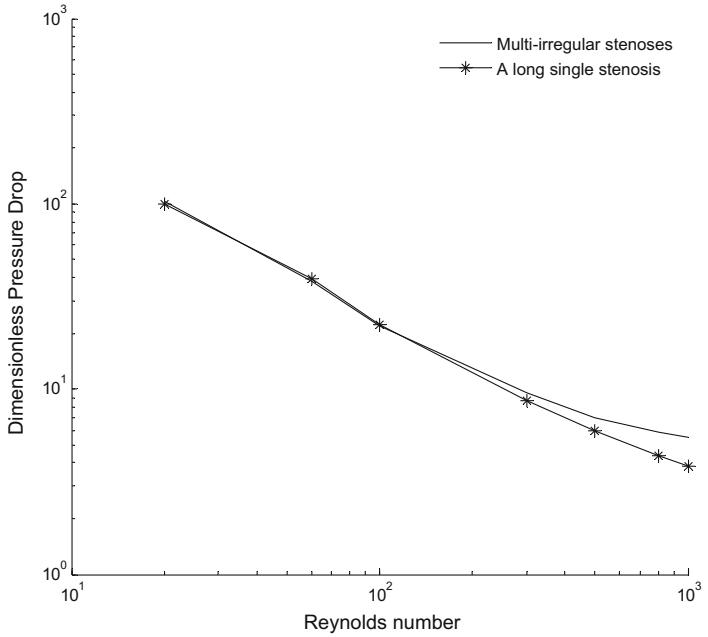

Fig. 6. Dimensionless pressure drop across multi-irregular stenoses and a long single stenosis of the same total length.

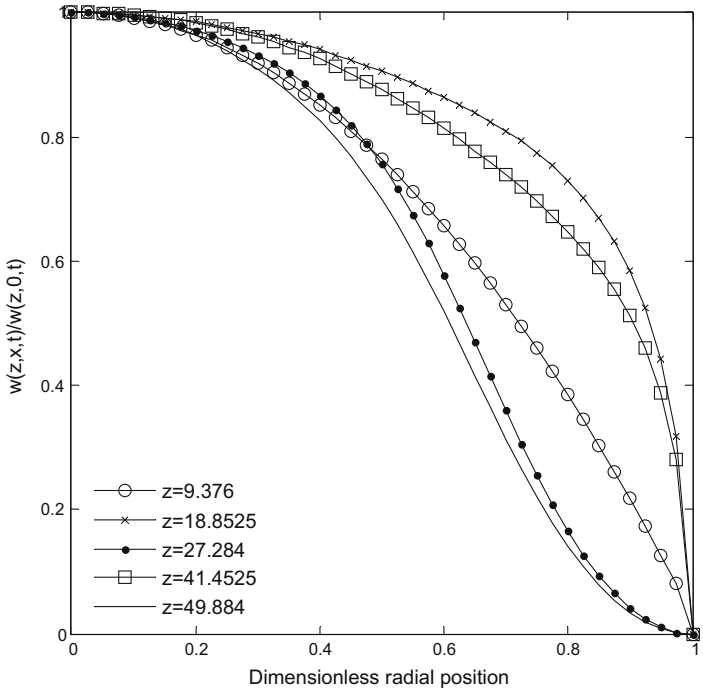

Fig. 7. Cross-sectional profiles of the axial velocity component corresponding to different axial positions in the multi-irregular stenoses at Re = 1000.

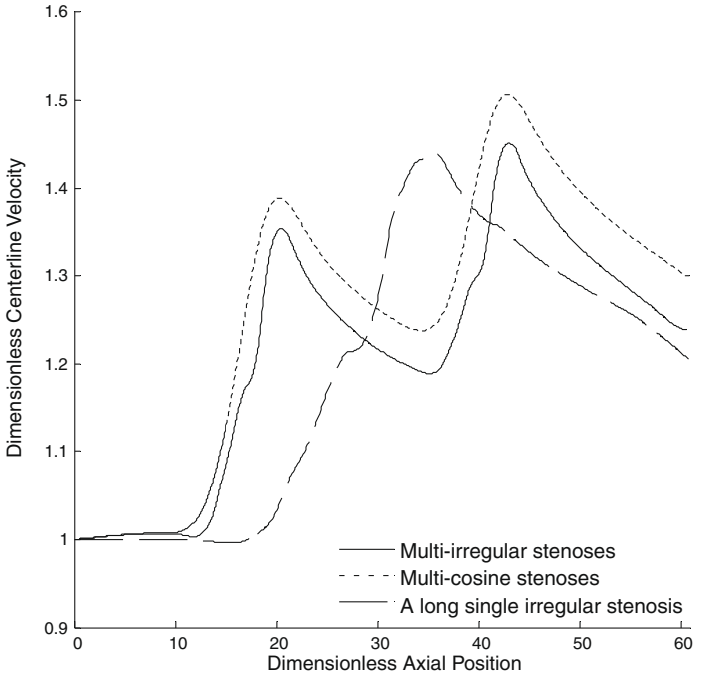

Fig. 8. Variation of the axial velocity component along the axis for each of the stenoses geometries at Re = 1000.

5.5. Wall shear stress

The flow separation points are observed when the shear stress at the wall changes its sign. The reattachment points followed by separation points occur when the wall shear stress changes its sign again.

Table 2
A critical Reynolds number.

Model of stenosis	Critical Reynolds number
Multi-irregular	450
Multi-cosine stenoses	620
A long single-irregular	910

The narrowest passage of all the outlines of the multi-cosine, multi-irregular stenoses and a long single irregular stenosis give rise to higher wall shear stress in the converging region of the stenosis, as portrayed in Figs. 9a and 9b for lower and higher Reynolds numbers respectively. The wall shear stress has been normalized by its magnitude corresponding to the Newtonian model in the unconstricted arterial tube far upstream of the stenosis. The present demonstration of the wall shear stress is compared with those of Johnston and Kilpatrick [5], Andersson et al. [6], Yakhot et al. [7] and Sariffudin et al. [15] for a single irregular stenosis and is found to have an excellent agreement with them. In the converging section of the stenosis, the irregular model predicts lower shear stresses, but at the narrowest point the values are much higher, followed by a change from higher shear stress to lower shear stress in the diverging sections of the irregular stenosis. The curves of Fig. 9a show no point of flow separation with a low Reynolds number (Re = 20). At Re = 1000, the stress magnitudes are greatly enhanced in general, and in particular the peak wall shear stresses corresponding to the all narrowest points. Multi-irregular stenoses show larger separated region compared to a cosine-shaped stenosis and a long single irregular stenosis as depicted in Fig. 9b. Thus one may conclude that the effect of multi-irregular stenoses is more severe than multi-cosine stenoses and also a single irregular stenosis so far as flow separation is concerned.

5.6. Variations of the severity of the stenoses

According to the modern conception in the realm of stenotic flow phenomena, recirculation zones are usually observed in arteries which experience a high degree of occlusion in their lumen. To study the effects of a more severe stenosis, the original stenosis profile (48% areal occlusion) is modified to increase the severity of 74% areal occlusion maintaining the same general shape. The variations of the combinations of severity of multi-irregular stenoses profiles are shown in Fig. 10.

5.6.1. Wall shear stress for various severities

In Fig. 11, the wall shear stress distributions show a close reflection of the outline of the stenoses. The point where the maximum shear stress occurs lies at the narrowest cross-section. In Fig. 11a, the separated region only occurs at the downstream of the first stenosis at Re = 500. There is a rapid increase in wall shear stress upstream of the first stenosis, then after the critical height of stenosis, the wall shear stress decreases until separation occurs. In Fig. 11b, a larger separation region is

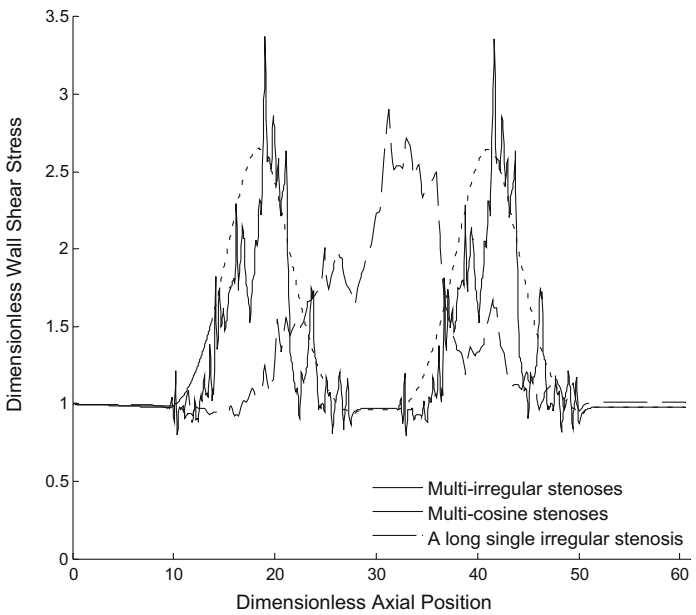

Fig. 9a. Variations of normalized wall shear stress through of each stenosis geometries at Re = 20.

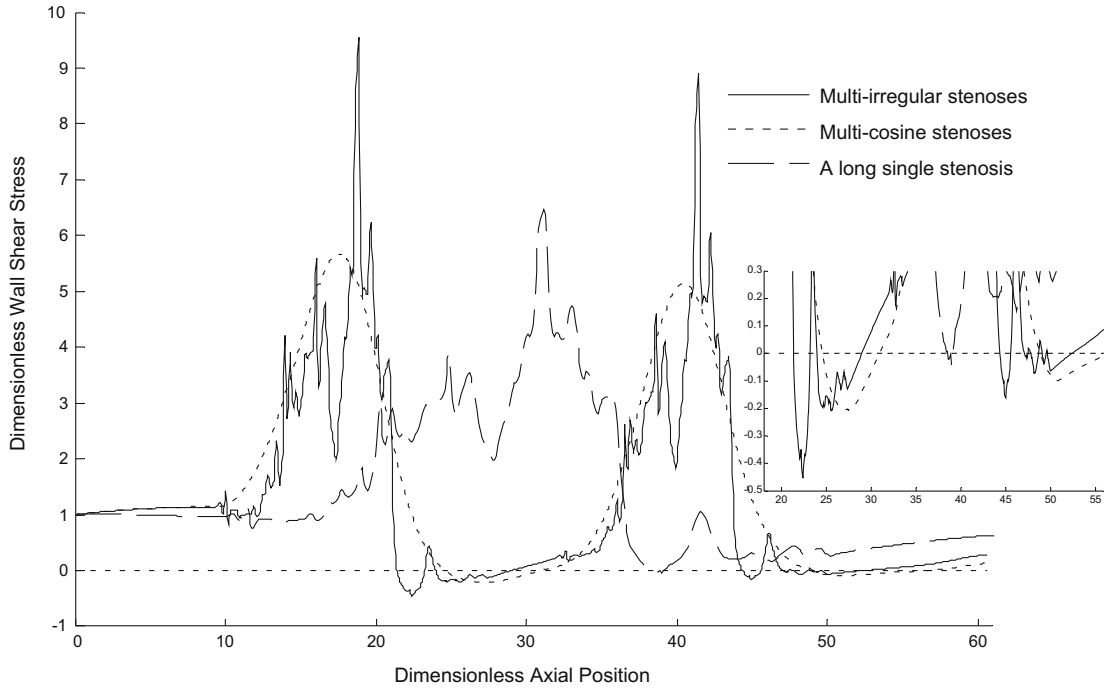

Fig. 9b. Variations of normalized wall shear stress through of each stenosis geometries at Re = 1000.

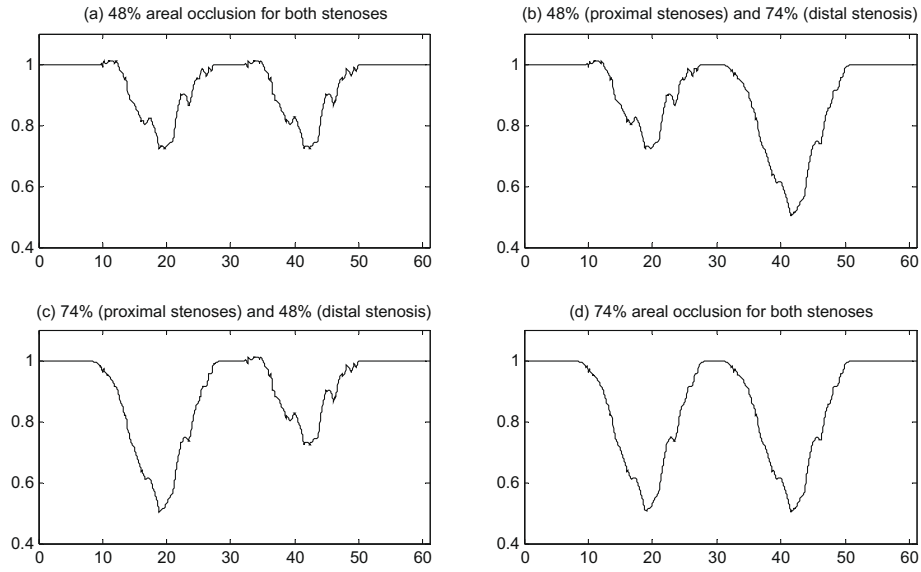

Fig. 10. Variations of the combinations of stenoses severity.

observed downstream of the distal stenosis. The maximum value of wall shear stress is at the critical height of the distal stenosis. From this figure one may note that the less severe stenosis does not affect the pattern of blood flow because the more severe stenosis dominates the flow field. From Fig. 11c, a large separated region is observed at the downstream of the proximal stenosis until the reattachment point occurs in the converging part of the distal stenosis. Fig. 11d depicts two large recirculation zones at Re = 500. Two larger separated regions are observed, the first is at downstream of the first stenosis until the upstream of the distal stenosis and the second is downstream of the distal stenosis. A large separation zone is observed in between the two identical stenoses having same severities. The peak of wall shear stress is at the critical height of both stenoses, with the values of wall shear stress at the first stenosis higher than at second stenosis.

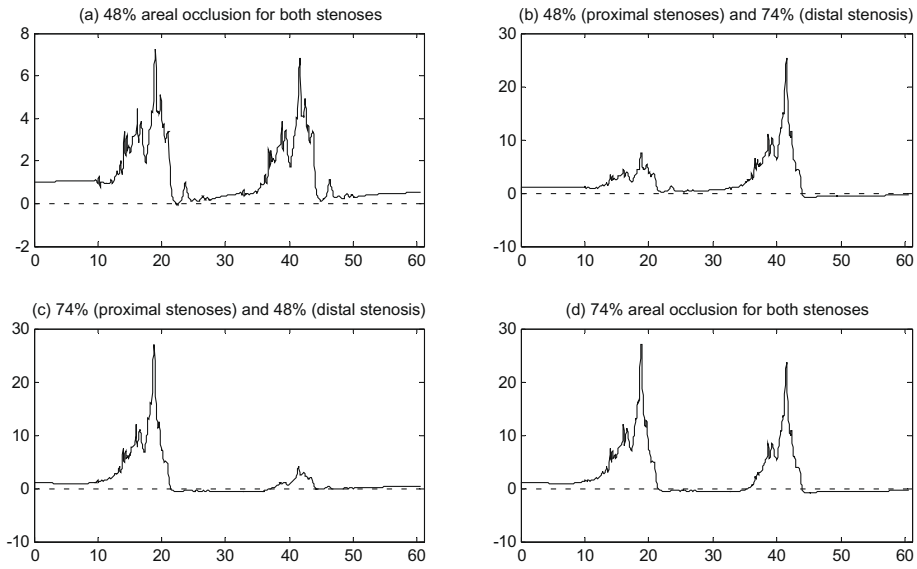

Fig. 11. The wall shear stress for the multi-irregular stenoses with the various severity combinations at Re = 500.

5.6.2. Streamline and vorticity

Instantaneous patterns of streamlines governing the flow of blood through the multi-irregular stenoses of different severity combination at Re = 500 is shown in Fig. 12. It is clearly seen that a large recirculation region develops at the downstream of more severe stenoses. In the case of 74% areal occlusion for both stenoses, recirculation regions are developed at two places, which are in between the two stenoses and in the diverging section of the second stenosis. One can see from the figures that fluid modeling structures replicate in detail the surface complex geometry.

From Fig. 13, vorticity contour has some interesting features and shows that when it crosses the narrowest section of the artery, vortices expand as the mean flow slightly decelerates. The line of vorticity moves towards the centerline of the tube resulting in a tortuous vorticity contour adjacent to the peak of the constriction. However, on the basis of our preliminary observations, it would seem that modeling a realistic geometry is important because surface irregularities may affect the dynamics of near-wall vortices. The correct prediction of the vortex dynamics might be important for estimating the near-wall residence times for blood cells. It is particularly relevant because it is now widely accepted that biological processes initiating atherosclerosis are strongly influenced by a combination of fluid and mechanical factors as propounded by Moore et al. [36].

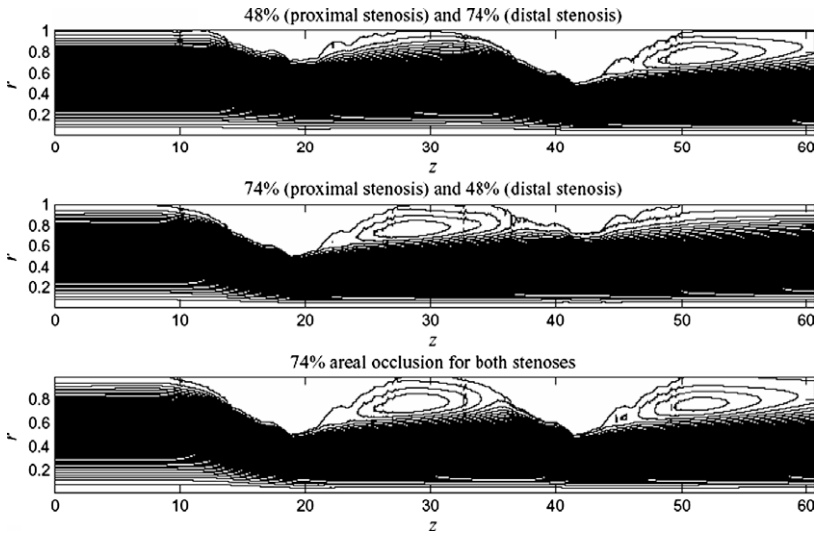

Fig. 12. Instantaneous patterns of streamlines for different combinations of stenoses severity.

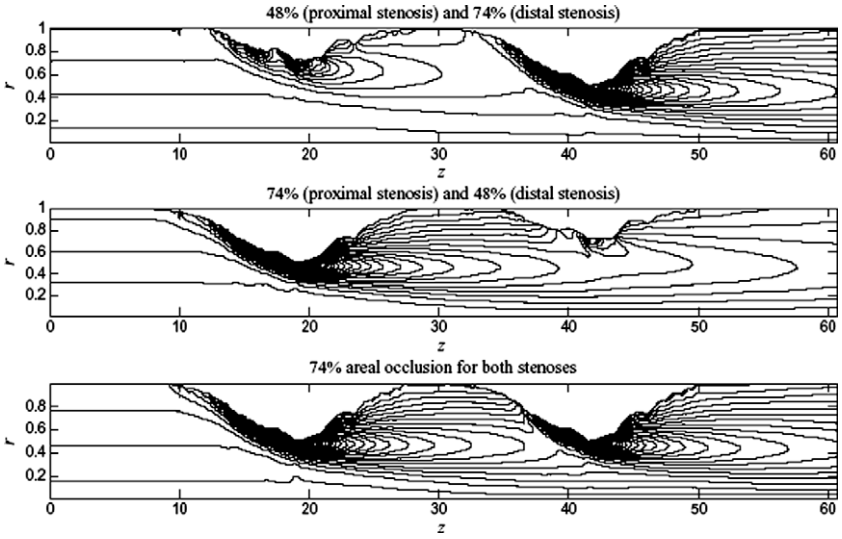

Fig. 13. Vorticity contour for the model of different combination of stenoses severity.

6. Conclusion

A two-dimensional axisymmetric mathematical model to study the characteristics of blood flow through an artery in the presence of a couple of stenoses with surface irregularities has been developed. The numerical simulation is primarily based on MAC method. The numerical stability and necessary convergence of the results obtained have been thoroughly examined and achieved with satisfactory level of accuracy within the specific computational domain of the present problem free from the choice of grid size. The behaviour of the computed results reveals the need of interpretation with proper justification and making scientific conclusions so that one can use the present findings into development of its future extension, if any. The novelty of the present study is the consideration of the Newtonian characteristics of the streaming blood past a flexible arterial segment containing a couple of irregular stenoses in its lumen. Since there is a coupling between the growth of the stenosis and the flow of blood in the artery each affecting other significantly and since the development of arterial coarctation usually of varied geometrical shapes, the choice of differently shaped stenoses models considered in the present study is of much importance in analyzing and estimating their influences on the flow phenomena.

One of the remarkable features is the occurrence of larger pressure drop experienced by the flowing blood over the entire range of Reynolds numbers in the cosine shaped stenoses model only relative to the irregular shaped model owing to the factor of larger area covering, however, a couple of irregular stenoses model experiences higher resistance to flow for $Re > 100$ than a long single irregular model (cf, Fig. 6).

Moreover, in the pattern of wall shear stress, the flow separation does occur for large Reynolds number in case of a long single irregular stenosis model. It is important to record that the multiple stenoses as well as their surface roughness prompt an early separation of flow (cf. Table 2).

The major limitation of the present study include the consideration of the arterial wall as a thin moving wall and the chosen sites of the stenoses in the arterial lumen. It has been speculated that the atherosclerotic lesions are preferentially occurred in arteries and arterioles in regions of high curvatures where there are bifurcations and junctions, the critical sites where there would be major changes in fluid loading on the vessel walls. Heterogeneity of vascular wall and non-Newtonian rheology of the streaming blood may certainly play important roles for the further development of the present investigation. Any development of the future extension of the present investigation in order to get away these limitation can be made successfully, however complex it may be, based on the present findings so that the model refinement analysis shall continue to achieve results closer to the real situation.

Acknowledgements

The final form of the paper owes much to the helpful suggestions of the referees, whose careful scrutiny we are pleased to acknowledge. The second author acknowledges the financial assistance in part from the Special Assistance Programme (Grant No. F. 510/8/DRS/2004 (SAP-I)) sponsored by University Grants Commission (UGC), New Delhi, India. Part of this work carried out at the Department of Mathematics, Visva-Bharati, India and Griffith University, Australia. The first author acknowledges the financial support provided by the Public Services Department of Malaysia and Universiti Teknologi Malaysia which enabled her to visit Australia and India to carry out the present research.

Appendix

$$A_{i,j} = \frac{x_{lj}R^k_{li}}{\Delta z_i \Delta zt} + \frac{x_{lj}R^k_{li}}{\Delta z_i \Delta zb} + \frac{x_j}{R^k_{li}\Delta x^2} + \frac{x_{j-1}}{R^k_{li}\Delta x^2},$$

$$B_{i,j} = -\frac{x_{lj}R^k_{li}}{\Delta z_i \Delta zt}, \quad C_{i,j} = -\frac{x_{lj}R^k_{li}}{\Delta z_i \Delta zb}, \quad D_{i,j} = \frac{x^2_{lj}R^k_{li}}{4\Delta x \Delta z_i}\left(\frac{\Delta z_{i+1}}{R^k_i \Delta zt}\left(\frac{\partial R}{\partial z}\right)_i - \frac{\Delta z_{i-1}}{R^k_{i-1}\Delta zb}\left(\frac{\partial R}{\partial z}\right)^k_{i-1}\right) - \frac{x_j}{R^k_{li}\Delta x^2},$$

$$E_{i,j} = \frac{x^2_{lj}R^k_{li}}{4\Delta x \Delta z_i}\left(\frac{\Delta z_{i+1}}{R^k_i \Delta zt}\left(\frac{\partial R}{\partial z}\right)^k_i - \frac{\Delta z_{i-1}}{R^k_{i-1}\Delta zb}\left(\frac{\partial R}{\partial z}\right)^k_{i-1}\right) - \frac{x_{j-1}}{R^k_{li}\Delta x^2}, \quad F_{i,j} = \frac{x^2_{lj}R^k_{li}}{4R_i \Delta x \Delta zt}\left(\frac{\partial R}{\partial z}\right)^k_i,$$

$$G_{i,j} = -F_{i,j}, \quad H_{i,j} = \frac{x^2_{lj}R^k_{li}}{4R^k_{i-1}\Delta x \Delta zb}\left(\frac{\partial R}{\partial z}\right)^k_{i-1}, \quad S_{i,j} = -H_{i,j},$$

where $\Delta zt = 0.5(\Delta z_i + \Delta z_{i+1})$ and $\Delta zb = 0.5(\Delta z_i + \Delta z_{i-1})$.

References

[1] L.H. Back, Y.I. Cho, D.W. Crawford, R.F. Cuffel, Effect of mild atherosclerosis on flow resistance in a coronary artery casting of man, ASME J. Biomech. Eng. 106 (1984) 48–53.
[2] R.M. Nerem, W.A. Seed, An in vivo study of aortic flow disturbances, Cardiovas. Res. 106 (1972) 1–14.
[3] E. Speir, R. Modali, E.S. Huang, M.B. Leon, F. Shawl, T. Finkel, S. Epstine, Potential role of human cytomegalovirus and p53 interaction in coronary restenosis, Science 265 (1994) 391–394.
[4] D. Liepsch, An introduction to biofluid mechanics: basic models and application, J. Biomech. 35 (2002) 415–435.
[5] P.R. Johnston, D. Kilpatrick, Mathematical modeling of flow through an irregular arterial stenosis, J. Biomech. 24 (1991) 1069–1077.
[6] H.I. Andersson, R. Halden, T. Glomsaker, Effects of surface irregularities on flow resistance in differently shaped arterial stenoses, J. Biomech. 33 (2000) 1257–1262.
[7] A. Yakhot, L. Grinberg, N. Nikitin, Modelling rough stenoses by an immersed-boundary method, J. Biomech. 38 (2005) 1115–1127.
[8] S. Chakravarty, P.K. Mandal, Sarifuddin, Effect of surface irregularities on unsteady pulsatile flow in a compliant artery, Int. J. Nonlinear Mech. 40 (2005) 1268–1281.
[9] A.K. Politis, G.P. Stavropoulos, M.N. Christolis, P.G. Panagopoulos, N.S. Vlachos, N.C. Markatos, Numerical modeling of simulated blood flow in idealized composite arterial coronary grafts: steady state simulations, J. Biomech. 40 (2007) 1125–1136.
[10] A.K. Politis, G.P. Stavropoulos, M.N. Christolis, P.G. Panagopoulos, N.S. Vlachos, N.C. Markatos, Numerical modelling of simulated blood flow in idealized composite arterial coronary grafts: transient flow, J. Biomech. 41 (2008) 25–39.
[11] A.K. Politis, G.P. Stavropoulos, F.G. Panagopoulos, N.S. Vlachos, N.C. Markatos, Numerical study of pulsatile flow in composite arterial coronary grafts, J. Biomech. 39 (suppl. 1) (2006) S402.
[12] E. Boutsianis, H. Dave, T. Frauenfelder, D. Poulikakos, S. Wildermuth, M. Turina, Y. Ventikos, G. Zund, Computational simulation of intracoronary flow based on real coronary geometry, Eur. J. Cardio-Thoracic Surg. 26 (2004) 248–256.
[13] Sarifuddin, S. Chakravarty, P.K. Mandal, H.I. Andersson, Mass transfer to blood flowing through arterial stenosis, J. Appl. Math. Phys. (ZAMP) 60 (2009) 299–323.
[14] S. Sarifuddin, P.K. Chakravarty, Mandal, Effect of heat and mass transfer on non-Newtonian flow-links to atherosclerosis, Int. J. Heat Mass Transfer, 52 (2009) 5719–5730.
[15] Sarifuddin, S. Chakravarty, P.K. Mandal, G.C. Layek, Numerical simulation of unsteady generalized Newtonian blood flow through differently shaped distensible arterial stenoses, J. Med. Eng. Tech. 32 (2008) 385–399.
[16] P.K. Mandal, S. Chakravarty, A. Mandal, Numerical study on the unsteady flow of non-Newtonian fluid through differently shaped arterial stenoses, Int. J. Comput. Math. 84 (2007) 1059–1077.
[17] B.D. Seeley, D.F. Young, Effect of geometry on pressure losses I models of arterial stenoses, J. Biomech. 9 (1976) 439–448.
[18] N. Talukder, P.E. Karayannacos, R.M. Nerem, J.S. Vasko, An experimental study of the fluid dynamics of multiple noncritical stenoses, J. Biomech. Eng. 99 (1977) 74–82.
[19] S.C.V. Dreumel, G.D.C. Kuiken, Steady flow through a double converging–diverging tube model for mild coronary stenoses, ASME J. Biomech. Eng. 111 (1989) 212–220.
[20] D. Kilpatrick, S.D. Webber, J.-P. Colle, The vascular resistance of arterial stenoses in series, Angiol. 41 (1990) 278–285.
[21] K.L. Gould, K. Lipscomb, Effects of coronary stenoses on coronary flow reserve and resistance, Am. J. Cardiol. 34 (1974) 48–55.
[22] H.N. Sabbah, P.D. Stein, Hemodynamics of multiple versus single 50 percent coronary arterial stenoses, Am. J. Cardiol. 50 (1982) 276–280.
[23] W.W. Nichols, M.F. O'Rourke, C. Hartley, McDonald's Blood Flow in Arteries – Theoretical, Experimental and Clinical Principles, fourth ed., Oxford University Press, Inc., New York, 1998.
[24] T. Fukushima, T. Azuma, T. Matsuzawa, Numerical analysis of blood flow in the vertebral artery, ASME J. Biomech. Eng. 104 (1982) 143–147.
[25] P.R. Johnston, D. Kilpatrick, Mathematical modeling of paired arterial stenoses, Proc. Comput. Cardiol. (1990) 229–232.
[26] K.C. Ang, J. Mazumdar, Mathematical modeling of triple arterial stenoses, Aust. Phys. Eng. Sci. Med. 18 (1995) 89–94.
[27] F.A.L. Dullien, M.I.S. Azzam, Flow rate-pressure gradient measurements in periodically non-uniform capillary tubes, AIChE J. 19 (1973) 222–229.
[28] C. Bertolotti, Z. Qin, B. Lamontagne, L.-G. Durand, G. Soulez, G. Cloutier, Influence of multiple stenoses on echo-Doppler functional diagnosis of peripheral arterial disease: a numerical and experimental study, Ann. Biomed. Eng. 34 (2006) 564–574.
[29] N. Mustapha, S. Chakravarty, P.K. Mandal, N. Amin, Unsteady response of blood flow through a couple of irregular arterial constrictions to body acceleration, J. Mech. Med. Biol. 8 (2008) 395–420.
[30] N. Mustapha, S. Chakravarty, P.K. Mandal, N. Amin, Unsteady magnetohydrodynamic blood flow through irregular multi-stenosed arteries, Comput. Biol. Med., published online.
[31] N. Mustapha, P.K. Mandal, I. Abdullah, N. Amin, T. Hayat, Numerical simulation of generalized Newtonian blood flow past a couple of irregular arterial stenoses, Numer. Methods Partial Differen. Equat., (2009) in press.
[32] A.A. Amsden, F.H. Harlow, The SMAC method: a numerical technique for calculating incompressible fluid flow, Los Alamos Scientific Lab, Report LA-4370, Los Alamos, 1970.
[33] G. Markham, M.V. Proctor, Modifications to the two-dimensional incompressible fluid flow code ZUNI to provide enhanced performance, C.E.G.B. Report TPRD/L/0063/M82, 1983.
[34] J.E. Welch, F.H. Harlow, J.P. Shannon, B.J. Daly, The MAC method, Los Alamos Scientific Lab, Report LA-3425, Los Alamos, 1996.
[35] G.A. Johnson, H.S. Borovetz, J.L. Anderson, A model of pulsatile flow in uniform deformable vessel, J. Biomech. 25 (1992) 91–100.
[36] J.A. Moore, D.A. Steiman, D.W. Holdsworth, C.R. Ethier, Accuracy of computational hemodynamics in complex arterial geometries reconstructed from magnetic resonance imaging, Ann. Biomed. Eng. 27 (1999) 32–41.